Batteries & Supercaps

Research Article
doi.org/10.1002/batt.202400580

Chemistry Europe
European Chemical Societies Publishing

www.batteries-supercaps.org

Atomistic Transport Mechanisms in Lithium Salt-Doped Ionic Covalent Organic Framework Electrolytes

Lei Cheng,[a] Yanhao Deng,[b, c] Jun Huang,[d] Zhengyang Zhang,[b] Huanan Duan,*[a] Yoonseob Kim,*[d, e] and Yanming Wang*[b, f]

Ionic covalent organic frameworks (iCOFs) have garnered significant attention as potential single-ion conductive solid-state electrolytes, where researchers have made substantial efforts in designing iCOF-based composites, aiming to improve their intrinsic low conductivity. One successful case is to fill iCOF channels with lithium salts, such as lithium bis(trifluoromethanesulfonyl)imide (LiTFSI). However, the ion transport mechanisms in these composite electrolytes are still largely unknown, hindering their further improvement. Here molecular dynamics simulations were employed to systematically predict the ion diffusivity in iCOF (e.g., TpPa-SO_3Li COF)-LiTFSI composite electrolytes with varying LiTFSI compositions at different temperatures. A positive correlation was observed between Li^+ diffusivity and LiTFSI:iCOF ratio, which was also verified by our experiments. Interestingly, the Li^+ diffusion energy barrier obtained by the Arrhenius equation exhibited nearly no dependency on the LiTFSI concentration, indicating the importance of temperature-insensitive microstructural-related factors. Radial distribution functions revealed that with a higher LiTFSI proportion, the coordination number of SO_3^- decreases, while that of $TFSI^-$ increases, suggesting a competition between these two species in the Li^+ solvation shell. Furthermore, configurational entropy and bond orientational order parameter calculations examined the degree of disorder in the Li^+ solvation structure. These results should improve our mechanistic understanding of iCOF-based electrolytes.

Introduction

Lithium-ion batteries (LIBs) are a type of rechargeable batteries that use lithium ions (Li^+) as the primary charge carriers, representing a mainstream electrochemical energy storage technology.[1] Since their commercialization in the 1990s, lithium-ion batteries have garnered immense attention and are considered a significant milestone in the development of the renewable energy industry.[2] Despite their successful commercialization, the continuous advancement of everyday devices demands ever-improving battery performance. Presently, commercial lithium-ion batteries predominantly use liquid electrolytes, posing severe challenges in terms of safety and energy density.[3]

One of the plausible solutions is lithium metal batteries (LMBs), featuring high-performance solid-state electrolytes and lithium metal anodes.[4] Such batteries promise extremely high energy densities while inherently mitigating safety risks associated with electrolyte leakage. Consequently, the development of high-performance solid-state electrolyte materials has become a critical issue in LMB research.[5,6] Common solid-state electrolytes include inorganic ones, represented by oxides and sulfides, and organic ones, represented by polymers. Compared to traditional liquid electrolytes (LEs), polymer electrolytes exhibit better lithium dendrite suppression and higher electrochemical stability. However, their lower room-temperature conductivity and Li^+ transference number are the main drawbacks that constrain their applicability. In contrast, inorganic solid electrolytes have a more pronounced ability to suppress lithium dendrites, offering higher ionic conductivity and Li^+ transference numbers compared to polymer electrolytes. Nevertheless, further improvements are needed in terms of electrochemical stability and interfacial contact performance.[7] This motivates the invention of emerging new solid-state electrolytes, such as covalent organic frameworks (COFs), which have shown tremendous potential.[8,9]

COFs are a class of porous crystalline polymers, formed by reversible reactions between organic molecules, creating highly stable covalent bonds[10] The first COF, based on boronic acid, was reported by Yaghi's research group in 2005, formed through the self-condensation of boronic acids.[11] The rapid development of ionic covalent organic frameworks (iCOFs) began with the introduction of spiroborate bonds, enabling Li^+

[a] L. Cheng, H. Duan
School of Materials Science and Engineering, Shanghai Jiao Tong University, Shanghai 200240, P. R. China
E-mail: hd1@sjtu.edu.cn

[b] Y. Deng, Z. Zhang, Y. Wang
Shanghai Jiao Tong University Joint Institute, University of Michigan, Shanghai Jiao Tong University, Shanghai 200240, P. R. China
E-mail: yanming.wang@sjtu.edu.cn

[c] Y. Deng
Department of Materials Science and Engineering, National University of Singapore, Singapore 117575, Singapore

[d] J. Huang, Y. Kim
Department of Chemical and Biological Engineering, The Hong Kong University of Science and Technology, Hong Kong SAR, P. R. China
E-mail: yoonseobkim@ust.hk

[e] Y. Kim
Energy Institute, The Hong Kong University of Science and Technology, Hong Kong SAR, China

[f] Y. Wang
Future Battery Research Center, Global Institute of Future Technology, Shanghai Jiao Tong University, Shanghai 200240, P. R. China

Supporting information for this article is available on the WWW under https://doi.org/10.1002/batt.202400580

conduction.[12] iCOFs, incorporating ionic functional groups within their frameworks, exhibit significant potential in energy devices, especially as solid-state electrolytes (SSEs) in LMBs.[13] This is attributed to their well-defined nanoscopic channels derived from highly crystalline structures, facilitating efficient ion conduction.[14] Depending on the type of ionic functional groups, iCOFs are classified as cationic or anionic.[15] Cationic iCOFs lack mobile cations and require the addition of extra cations within the framework, resulting in lower cation transference numbers.[16,17] In contrast, anionic iCOFs enable cation migration within the channels, exhibiting ionic conductivities ranging from 10^{-7} to 10^{-4} S/cm and high electrochemical stability.[18] In general, pure anionic iCOFs are intrinsic single-ion conductors but with relatively low conductivities. Besides modifying the topological structures and functional groups of iCOFs, developing iCOF-based composite electrolytes is an effective approach to enhance their performance.[19,20]

In early studies on COF-based composite electrolytes, researchers mixed electrically neutral COFs with polymer electrolytes. Although their conductivity was somewhat improved, the issue of low ionic transference numbers in polymer electrolyte systems remained unresolved. Chen et al.[21] compared the ionic conductivity characteristics among composite electrolytes based on neutral COFs, cationic iCOFs, and anionic iCOFs, finding that the anionic iCOF-based composite electrolytes exhibited the highest conductivity and ionic transference numbers. Guo et al.[22] synthesized a high-conductivity, high-Li^+ transference number solid-state electrolyte by combining TpPa-SO_3Li (anionic iCOF), polymer ionic liquids, and LiTFSI in a specific ratio. On the theoretic side, molecular dynamics simulations revealed that small molecules like LiTFSI can diffuse into iCOF channels easily, whereas polymer chains will be kept outside the frame.[23] This alteration in ion transport properties within iCOF channels due to the insertion of LiTFSI may be crucial for the enhanced performance of composite electrolyte systems, though the underlying mechanisms require further systematic investigation. Multiscale simulation techniques, particularly first-principle calculations at the electronic scale and classical molecular dynamics (MD) simulations at the atomic scale, are playing a more critical role in understanding the microscopic behaviors in electrolyte systems.[24] Due to the relative scarcity of force field functions, most of the existing studies are based on the density functional theory (DFT) method, which can reveal ion migration pathways, migration energy barriers, and ion diffusion behaviors, but within a very short period of time (in the order of picoseconds) and at extremely high temperatures.[9,25] Obviously, for iCOF-based composite electrolytes, their complex amorphous configurations by nature require atomistic simulations at larger time and length scale, where classical MD appears to be more suitable.

In this work, we constructed atomistic configurations for iCOF/LiTFSI composite electrolytes with different composite ratios and performed MD simulations across a range of temperatures from 423 K to 498 K. As a model system for the iCOF, we chose TpPa-SO_3Li as this is one of the widely studied iCOF for battery applications. We systematically screened the ion transport properties of iCOF/LiTFSI composite electrolytes, by calculating the diffusion coefficients of Li^+ and $TFSI^-$ ions from mean square displacement (MSD) curves. In addition, the ion diffusion barriers were estimated by fitting the Arrhenius equation, to elucidate the underlying mechanisms of ion transport properties in this composite electrolyte system. The radial distribution functions (RDFs) and coordination numbers (CNs) further revealed that the addition of LiTFSI introduces the competition between SO_3^- and $TFSI^-$, effectively weakening the binding of SO_3^- to Li^+. Finally, configurational entropy and bond orientational order parameters (BOO) were utilized to quantitatively assess the degree of disorder in the solvation structure, jointly characterizing the complex solvation structures of Li^+ within the iCOF channels.

Results and Discussion

The ion transport properties obtained from molecular dynamics simulations are shown in Figure 1. Considering the significant differences in the number of Li^+ and $TFSI^-$ ions in the composite electrolyte systems at different LiTFSI ratios, we used the diffusion coefficient as an indicator of ionic conductivity (that is explicitly proportional to Li^+ concentration). Taking the MSD and diffusion coefficient trends of Li^+ and $TFSI^-$ with different LiTFSI:iCOF ratios at a fixed temperature (473 K) as an example (Figure 1b and c), it can be seen that at lower LiTFSI:iCOF ratios, the values of diffusion coefficients are similar to those of $TFSI^-$. Compared to pure iCOFs, the addition of a small amount of LiTFSI slightly enhances the ion diffusion of Li^+. When the LiTFSI:iCOF ratio increases to 1:4, a significant difference appears in the diffusion coefficients between Li^+ and $TFSI^-$. As the LiTFSI:iCOF ratio further increases, the diffusion coefficient of Li^+ shows an upward trend, whereas the diffusion coefficient of $TFSI^-$ remains low and even shows a declining trend. At a ratio of 1:2, the diffusion coefficient of Li^+ is approximately five times higher than that of $TFSI^-$. Figure 1d shows the trend of Li^+ and $TFSI^-$ diffusion coefficients across all simulated temperatures. Detailed data have been provided in the Supporting Information (Table S2, Table S3). We found that at all calculated temperatures, the diffusion coefficients of Li^+ and $TFSI^-$ preserve the same trends. This reveals an intriguing phenomenon: the incorporation of LiTFSI into iCOF channels enhances the transport of Li^+ while suppresses the transport of $TFSI^-$. The different behavior of Li^+ and $TFSI^-$ is speculated to be related with the spatial confinement effect: that is, given the average size of iCOF channels is merely about 1–2 nm, one $TFSI^-$ molecule, which has a significantly larger volume than that of Li^+, is likely to receive greater resistance when traveling within the pore. Certainly, the above argument cannot explain the enhanced Li^+ ion conductivity, thus, our main target in the rest of the paper is to unravel the underlying mechanisms of Li^+ transport in the LiTFSI/iCOF composite electrolytes.

Li^+ ion conductivity improvement was verified by our experimentally synthesized composite electrolytes of TpPa-SO_3Li (iCOF) and LiTFSI. As shown in Figure 2, when the ratio of LiTFSI to iCOF was 1:2, the room-temperature conductivity of this electrolyte reached 0.083 mS/cm, representing a threefold

Research Article
doi.org/10.1002/batt.202400580

Chemistry Europe
European Chemical Societies Publishing

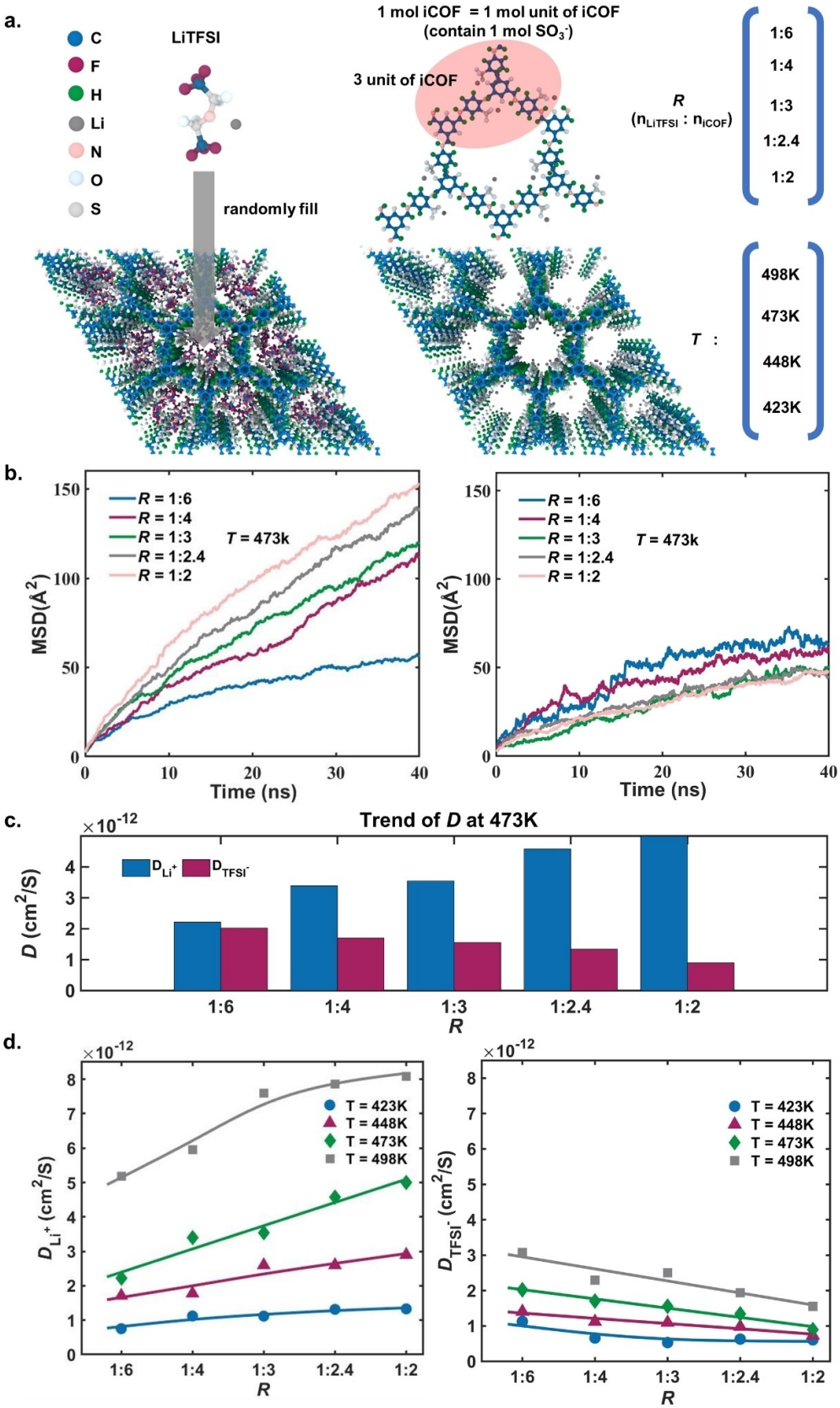

Figure 1. Ion transport properties at different composite ratios ($R = n_{LiTFSI} : n_{iCOF}$) and temperatures *T*. a, Representative configurations for molecular dynamic simulations of iCOF/LiTFSI composite electrolytes**. b**, Mean square displacement curves of Li^+ and $TFSI^-$ at 473 K. **c**, Diffusion coefficient trends of Li^+ and $TFSI^-$ for different composite ratios at 473 K. **d**, Diffusion coefficients of Li^+ and $TFSI^-$ for a set of composite ratios at various temperatures.

Research Article
doi.org/10.1002/batt.202400580
Chemistry Europe
European Chemical Societies Publishing

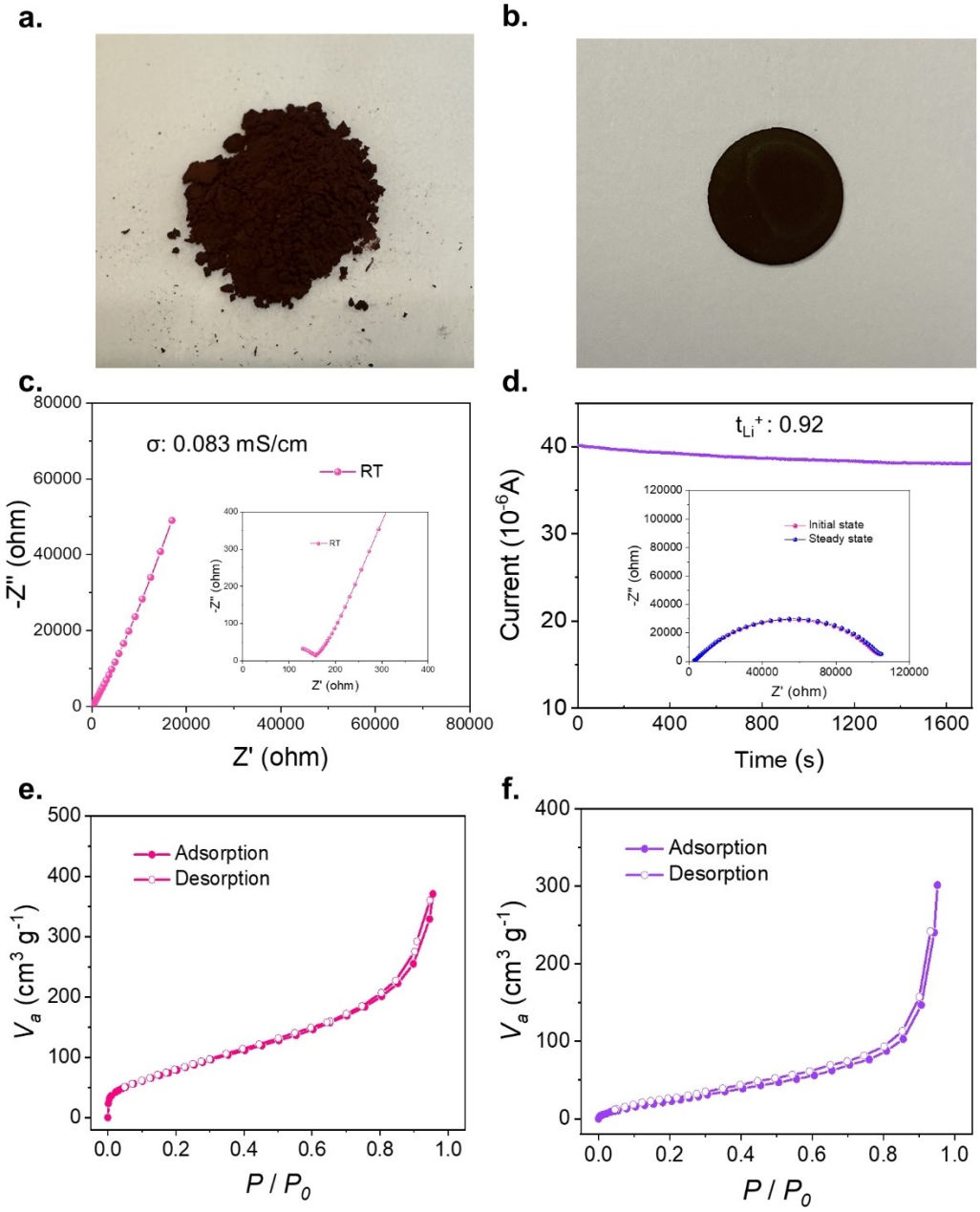

Figure 2. Experimental data of iCOF/LiTFSI composite electrolyte. a–b, iCOF/LiTFSI composite powder and solid electrolyte. **c**, Nyquist plots of electrochemical impedance spectroscopy (EIS) measurements at room temperature for TpPa-SO_3Li/LiTFSI Insets are zoomed-in Nyquist plots. **d**, Chronoamperometry profiles of Li | TpPa-SO_3Li/LiTFSI | Li symmetric cells, respectively. Insets are Nyquist plots of EIS measurements before and after polarization. **e–f**, Nitrogen gas sorption isotherms measured at 77 K for TpPa-SO_3Li only and TpPa-SO_3Li/LiTFSI.

increase compared to that of pure iCOFs, while maintaining a high Li^+ transference number of 0.93. By comparing the specific surface area (V_a) of pure iCOF with that of the composite electrolyte, we found that V_a decreased from 316.2 m^2/g to 108.5 m^2/g, suggesting that LiTFSI molecules indeed filled the iCOF channels in the composite electrolytes,[23] validating one key assumption of our molecular dynamics model. The above experimental observations show good agreements with the MD predictions, serving as a strong validation of our model.

Adopting the Arrhenius equation to our MD data, we estimated the change in diffusion energy barriers of Li^+ and $TFSI^-$ with varying LiTFSI:iCOF ratios (Figure S7). As shown in Figure 3a, the diffusion coefficient data for ions at the same ratio but different temperatures were fitted into the Arrhenius equation. The slopes of the $\ln(D) - 1/T$ curves were used to calculate the ion diffusion barriers. From the trend of ion diffusion barriers with the LiTFSI composition, in Figure 3b, we found that in general the diffusion barrier of Li^+ is significantly higher than that of $TFSI^-$. The diffusion barrier of Li^+ only varies within a small range, and the diffusion barriers of both ions do not exhibit a monotonic trend consistent with their diffusion coefficients.

Research Article
doi.org/10.1002/batt.202400580
Chemistry Europe
European Chemical Societies Publishing

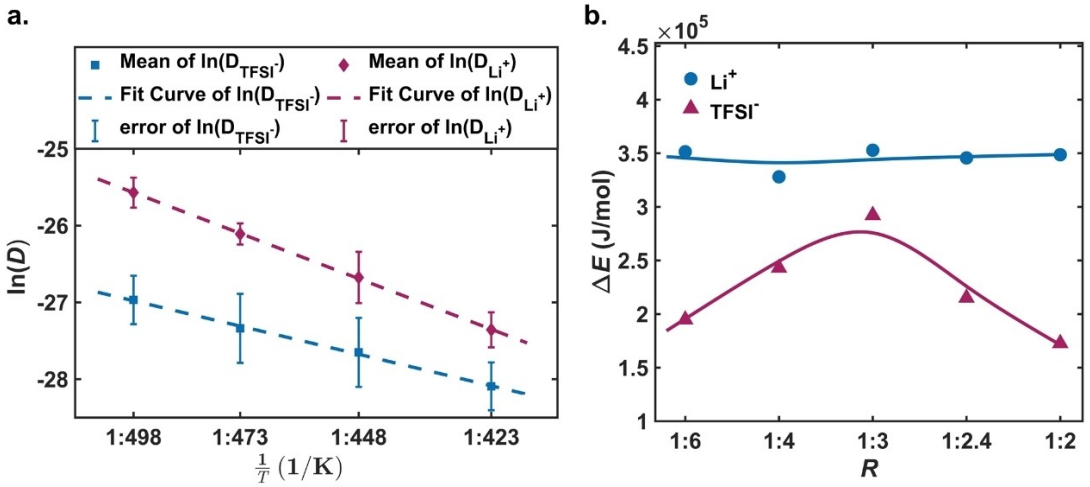

Figure 3. Calculation of energy barrier (ΔE). a, Linear relationship between ln(D) and 1/T. **b**, Variation of ΔE with R (n_{LiTFSI} : n_{iCOF}).

In a well-defined crystalline system, D_{Li^+} is often given by: $D_{Li^+} = A\exp\left(-\frac{\Delta E}{RT}\right)$, where ΔE is the activation energy for diffusion and A is a temperature-insensitive pre-exponential factor. Adopting a similar concept to the iCOF-based electrolyte (considering that certain periodicity can be found in COF), without loss of generality, the Li^+ diffusion coefficient $D_{Li^+} = D_0\exp\left(-\frac{\Delta G}{RT}\right) = D_0\exp\left(\frac{\Delta S}{R}\right)\exp\left(-\frac{\Delta H}{RT}\right)$, where ΔH, the enthalpy change, can be well related to ΔE, representing the temperature (T) dependency of D_{Li^+}. Since in our cases ΔE does not exhibit a strong correlation with the addition of LiTFSI (Figure 3b), the enhancement of D_{Li^+} must be related to the pre-factor of the above equation, i.e., the $D_0\exp\left(\frac{\Delta S}{R}\right)$ term. In other words, if we assume the factors such as Li^+ vibration frequencies and iCOF interlayer distances do not significantly vary, we speculate that very possibly the ΔS (entropy change) related contributions, e.g. the degree of disordering affected by the atomistic local environments, play a dominant role in determining the ion conductivity.

Thus, to construct a microscopic configuration perspective, we systematically studied the coordination environment of Li^+ using atomic trajectory data obtained from MD simulations. As shown in Figure 4a, the radial distribution functions (RDFs) of negatively charged atoms in the SO_3^- group and the $TFSI^-$ anion around Li^+ were calculated at different LiTFSI concentrations, revealing primary Li^+ binding sites: the two oxygen atoms in SO_3^-, and the nitrogen and oxygen atoms in $TFSI^-$. We then performed an in-depth comparative analysis of the RDFs of these four types of atoms in composite electrolytes with different LiTFSI:iCOF ratios (Figure 4b). Here we observed some common features: the width of the first peak in the RDFs for these four types of atoms did not change significantly with varying LiTFSI:iCOF ratios. However, as the LiTFSI proportion increased, the peak heights gradually decreased. And the peak positions in the RDFs for the two types of oxygen atoms in SO_3^- were slightly shifted to larger values.

The coordination number trends for these atoms indicate a decrease in the coordination number of atoms in SO_3^- and an increase in the coordination number of atoms in $TFSI^-$ (Figure 5a and b). Linking this observation with the Li^+ diffusivity change of the electrolyte system, it implies that with more LiTFSI salts being added, the competition between $TFSI^-$ and SO_3^-, consequently reducing the average number of Li^+ binding with SO_3^-, facilitates the dissociation of Li^+. In addition, the total coordination number of the first shell of negatively charged atoms exhibits an increasing trend, which may effectively provide more coordination sites for Li^+ to promote its migration.

To further verify the relationship of solvation structure with Li^+ ion transport, we computed the interaction energies between Li^+ and $TFSI^-$, SO_3^-, and all the anions in the system, averaging across all lithium ions. As shown in Figure 5c, in the iCOF/LiTFSI composite electrolyte, the interaction (attraction) energy between Li^+ and $TFSI^-$ increases as the LiTFSI/iCOF ratio rises. In contrast, the interaction energy between Li^+ and SO_3^- weakens, consistent with the coordination number calculations. This finding reinforces our understanding of the competitive interactions between $TFSI^-$ and SO_3^- for Li^+ binding. As a consequence, when LiTFSI concentration becomes higher, more intensive competition between $TFSI^-$ and SO_3^- facilitates the dissociation of Li^+, leading to an enhanced Li^+ diffusivity.

Figure 6a carefully examined the appearances of the RDF curves. With the increase in the ratio of LiTFSI to iCOFs, the curves exhibit similar shapes, with the first peak appearing between 2–3 Å. Specifically, the first minimum of the curves occurs around $r = 2.625$ Å for all cases. When r exceeds 10 Å, the value of $g(r)$ gradually converges to 1. These numbers provide useful inputs for the subsequent calculations of configurational entropy S_{Config}, for further quantification of the local microscopic environment of Li^+ solvation. From the RDF data, the configurational entropy S_{Config}, as a major component of the system's total entropy, can be approximated by the following equation:

Research Article
doi.org/10.1002/batt.202400580
Chemistry Europe
European Chemical Societies Publishing

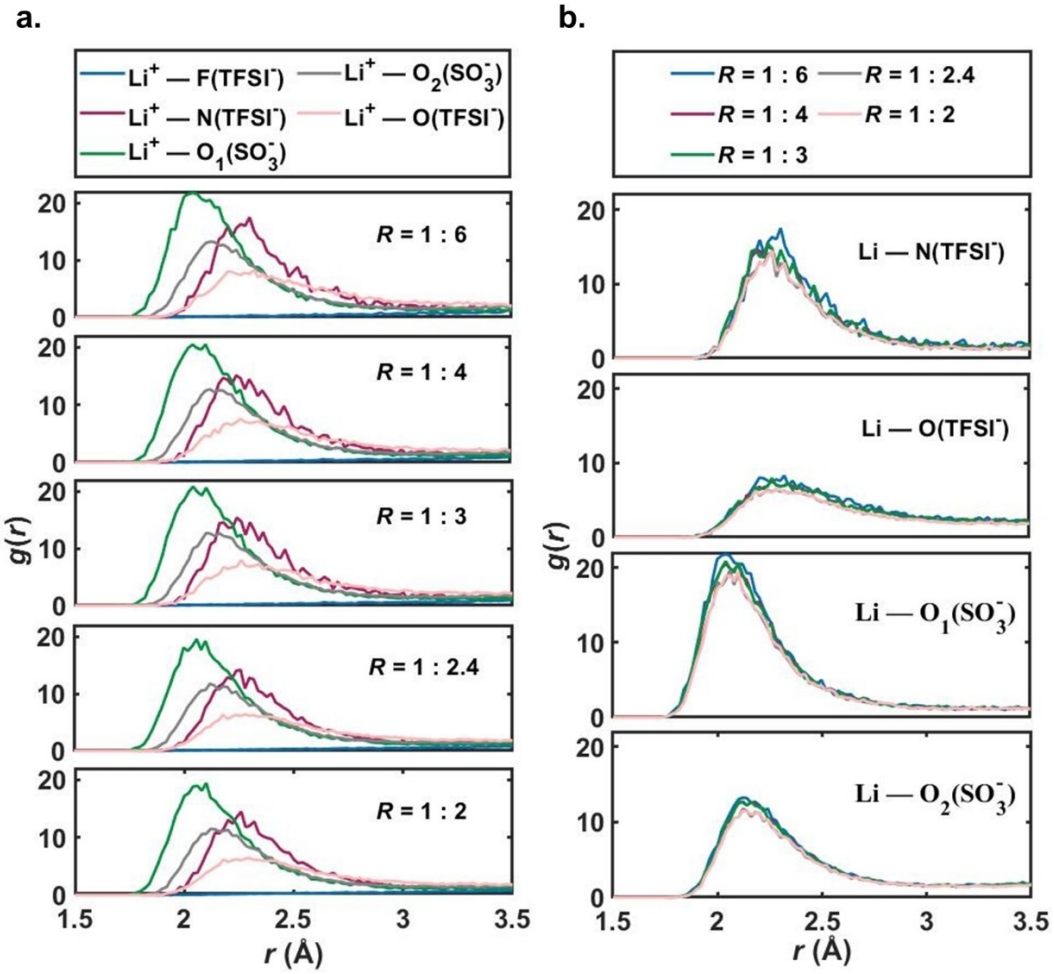

Figure 4. Partial Radial distribution function (RDF) analysis. a, Partial RDFs for Li to negatively charged atoms in SO_3^- and $TFSI^-$. **b**, Comparison of RDFs between the same atoms in electrolyte systems with different LiTFSI:iCOF ratios.

$$S_{\text{Config}} = -2\pi\rho k_B \int_0^{r_c} [g(r)\ln(g(r) - g(r) + 1)]r^2 dr$$

where k_B is the Boltzmann constant, and the cutoff radius r_c for the integral is typically chosen as the value of r where $g(r)$ converges to 1.[26] In our case, it can be seen that $g(r)$ tends to converge to 1 when r is greater than 10 Å; therefore, we set the cutoff at a larger value, 15 Å, to ensure the accuracy of the calculation for every simulation scenario. For each LiTFSI:iCOF ratio at 473 K, we randomly selected 20 frames from three independent MD trajectories to estimate the configurational entropy, and then made an average from those values for a better statistical representation. It is important to note that for ion migration, the configuration within the first shell plays a significant role. Thus, we also calculated the configurational entropy within the first shell. The results shown in Figure 6b indicate that as the LiTFSI concentration increases, the overall entropy of the material increases, consistent with our hypothesis on the ΔS; but the entropy within the first shell exhibits an opposite trend, suggesting that the solvation structure may become more ordered in the radial direction when the SO_3^- competes with the $TFSI^-$

To further understand solvation behaviors of Li^+ (besides the configurational entropy analysis along the radial direction), we conducted an in-depth investigation on the solvation configuration of Li^+ regarding the rotational degree of freedom. We employed bond orientational order parameters (BOO) and convoluted BOO parameters to quantitatively characterize the local structural arrangement of atoms. As shown in Figure 7, we calculated three different parameters. q_{12} considered the atoms in the first coordinate shell, while $\overline{q}_{12}$ and $\overline{Q}_{12}$ included the information from the second solvation shell by applying different convolute methods. With the proportion of LiTFSI increases, the distributions of these parameters become closer to the disordered state (labeled as AM in Figure 7). This implies that the configuration entropy in the rotational degree also tends to slightly increase with the addition of LiTFSI. In Figure 6, configurational entropy is derived from the metrics of pair distances, whereas in Figure 7, the BOO parameters are calculated solely from bond orientation, in principle orthogonal to radial distribution. Together, these metrics should provide comprehensive insights into the first coordination shell (in the

Research Article
doi.org/10.1002/batt.202400580
Chemistry Europe
European Chemical Societies Publishing

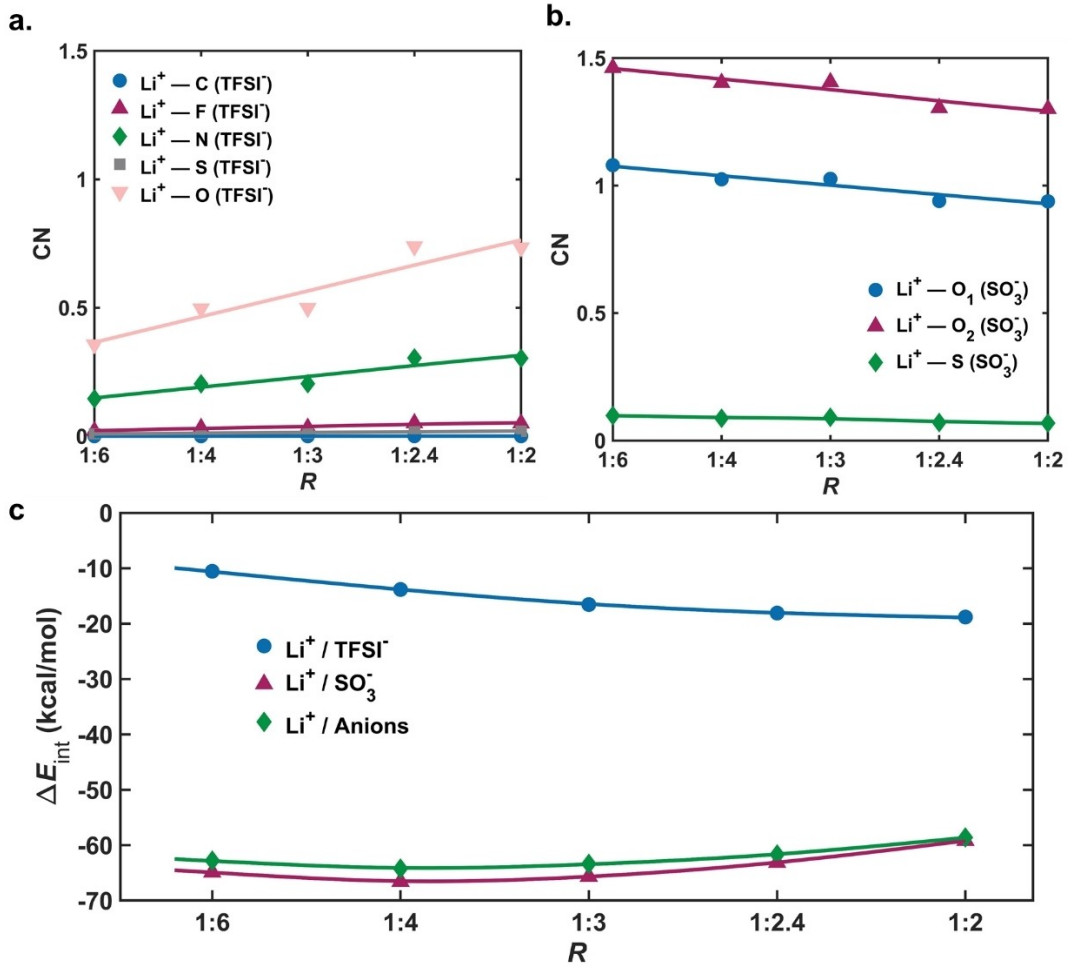

Figure 5. Variation in coordination number (CN) of Li^+ with atoms in SO_3^- and TFSI $^-$ anions across different material composition ratios. a, CN of Li^+ with atoms in $TFSI^-$. **b**, CN of Li^+ with atoms in SO_3^-. **c**. Interaction energies between Li^+ and $TFSI^-$, SO_3^-, and all the anions respectively.

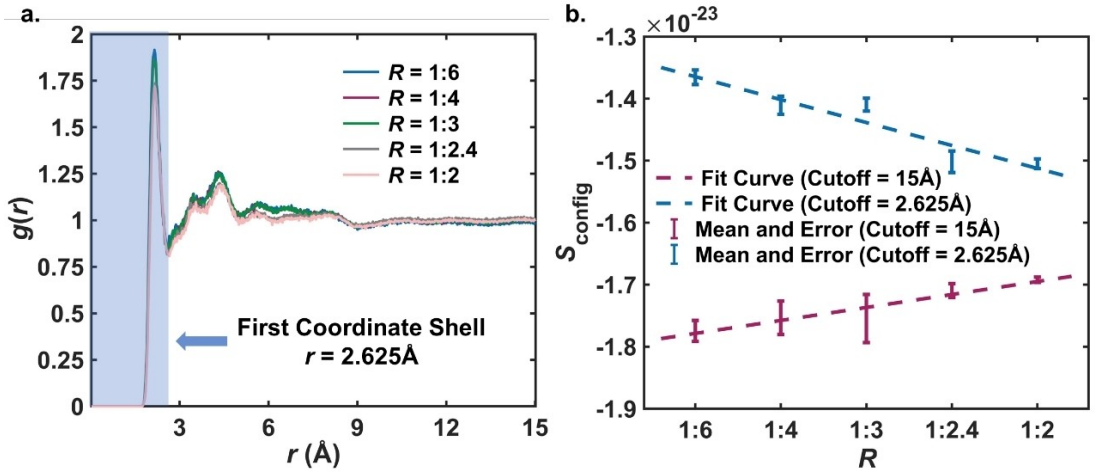

Figure 6. Radial distribution function (RDF) and Configuration entropy analysis. a, RDF for Li^+ with all types of atoms. **b**, Variation of configuration entropy with proportion.

radial and rotational directions). For mid-range atomic arrangements, encompassing the second coordination shell, the increase in structural disordering with higher LiTFSI concentration is also captured from both orientation and radial distribution analyses.

Research Article
doi.org/10.1002/batt.202400580
Chemistry Europe
European Chemical Societies Publishing

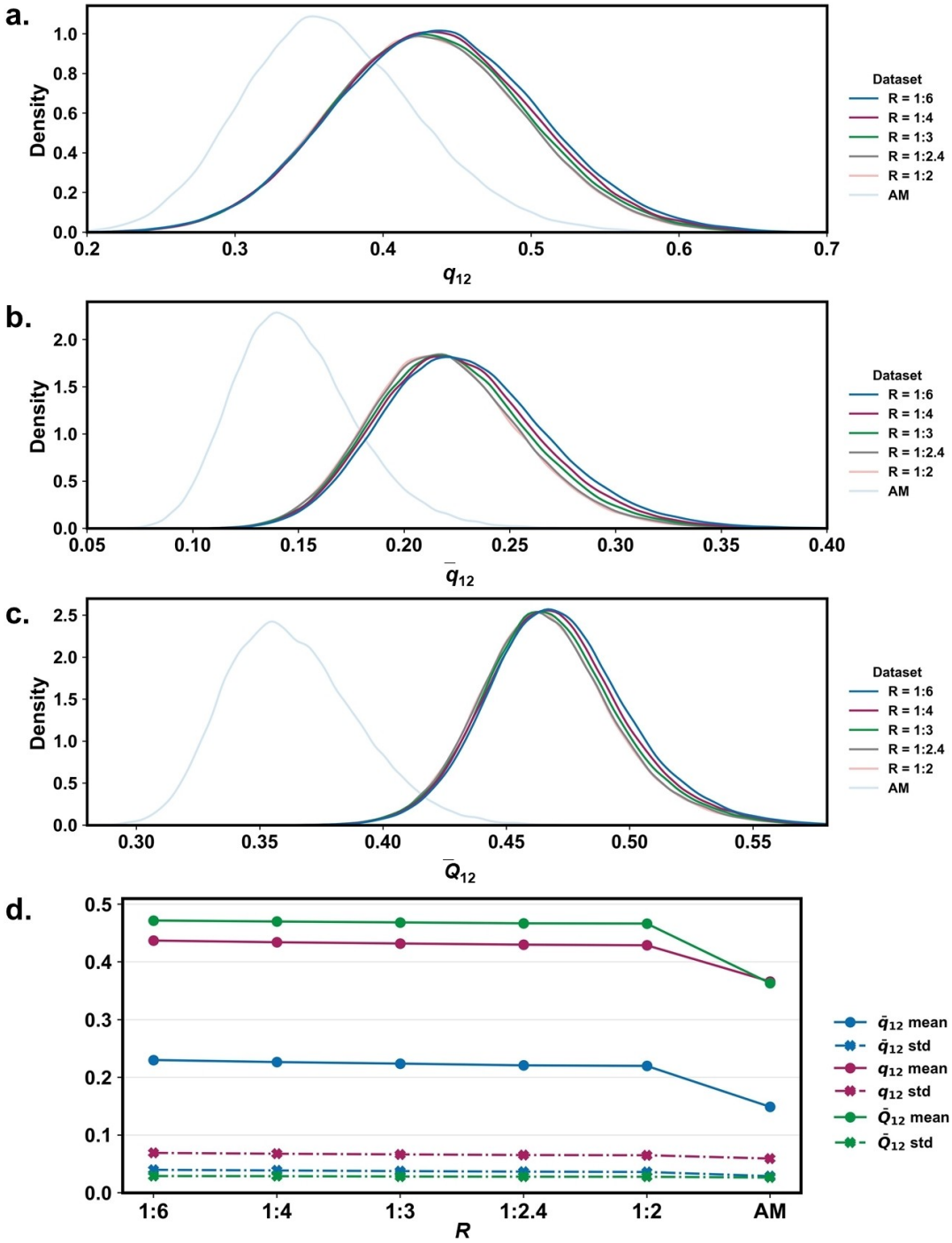

Figure 7. a–c: Distribution of parameters q_{12}, $\bar{q}_{12}$, $\bar{Q}_{12}$ on systems of different composite ratios and amorphous system. **d**, Mean value and standard deviation of the distributions of these parameters.

Conclusions

In this study, we employed molecular dynamics simulations for studying the iCOF/LiTFSI composite electrolytes at various temperatures and ratios, to reveal how the incorporation of LiTFSI facilitates ion transport within iCOF. It is observed that these iCOF channels filled with LiTFSI can rapidly conduct Li^+ while immobilizing $TFSI^-$, providing a promising direction toward high conductivity and high transference number in these composite electrolytes. The ion diffusion barrier calculations indicated that the entropy changes in the iCOF-based electrolyte systems seem more dominant in affecting ion diffusion, which are further examined by a series of analyses based on radial distribution function, configurational entropy and bond order orientational parameter. Our results demonstrate the importance of atomistic local environments in

affecting the ion transport of iCOF/LiTFSI composite electrolytes. The computational knowledge developed here should be applicable to other iCOF systems, including the ones with various ionic moieties, different pore sizes, and the third or fourth components in the composites. Overall, we believe that these findings should lay a solid foundation, for motivating the development of innovative iCOF-based electrolytes via tailoring the Li^+ solvation structure within iCOF channels.

Method

For experiments, TpPa-SO3Li (iCOF) is synthesized through a Schiff-base condensation reaction between 1,3,5-triformylphloroglucinol (Tp) and 1,4-phenylenediamine-2-sulfonic acid, followed by cation exchange from H^+ to Li^+. Key steps in the synthesis include (1) condensation reaction and (2) cation exchange. The Schiff-base condensation reaction between the aldehyde groups in Tp and the amine groups in the sulfonic acid-modified phenylenediamine forms the framework structure. After the COF formation, the cation exchange from H^+ to Li^+ takes place, enabling the material to facilitate lithium-ion conduction.

The composite electrolyte was synthesized by mixing LiTFSI and iCOF. LiTFSI is first dissolved in acetonitrile to form a homogeneous solution. Then iCOF powder is added to the LiTFSI solution, and the mixture is stirred thoroughly to ensure uniform dispersion of the iCOFs within the LiTFSI matrix. The mixture is subjected to solvent evaporation and drying processes, resulting in the formation of composite pellets (Figure 2a).

Molecular dynamics simulations for composite electrolytes with varying ratios at a series of temperatures were designed to systematically investigate the ionic conductivity characteristics and underlying mechanisms. For systems with the same ratio and temperature three independent simulations with randomly defined initial configuration were performed to randomize ion trajectories and reduce the impact of random errors. We defined 1 (mol of) iCOF framework repeating units with 1 (mol of) Li^+ as 1 (mol of) iCOF (Figure 1a). The base configurations of LiTFSI and iCOF were constructed in MedeA.[27] Taking into account the distribution of SO_3^- in the framework, the unit cell of the iCOF model consists of two layers of iCOF, with each layer composed of three repeat units of iCOF. For all MD simulations, a 3×3×6 supercell was used to ensure the statistical interpretability of the MD data (Figure S1). Stable configurations of pure iCOF were obtained after 1 ns of NVT simulation and 5 ns of NPT simulation. Initial configuration of iCOF/LiTFSI composite electrolyte was obtained by randomly filling the Li atoms and $TFSI^-$ molecules into the pores of iCOF. To minimize the occurrence of atomic distances being too close or overlapping, Latin hypercube sampling (LHS) was used to determine the spatial positions and orientations of LiTFSI within the stable iCOF channel configurations. LHS is a stratified sampling method. More specifically, before obtaining the atomic positions and spatial orientations of LiTFSI, the simulation space was partitioned into independent subspaces based on the probability distribution. Sampling was then performed within each subspace, significantly reducing the occurrence of atoms being too close or overlapping in the initial configurations. This approach prevents errors and computational crashes in subsequent simulations due to excessively large interatomic forces between atoms that are too close.[28]

According to experiments and DFT theoretical calculations, the interlayer spacing of TpPa-SO_3Li is 3.53 Å, and the channel diameter is approximately 11.8 Å.[9] The stable relaxed configuration of iCOF has a length of 40.12 Å in the direction of the pore extension, interlayer spacing is 3.34 Å, which is very close to the value from experiments and DFT calculation. Assuming a similar density to LiTFSI when filling the channels, each channel can accommodate approximately 12 to 13 LiTFSI molecules. More details can be found in the Supporting Information. To simulate the actual distribution of LiTFSI within the channels, the model with the highest composite ratio (1 : 2) includes 18 LiTFSI molecules randomly distributed within each channel. Though, this value is slightly higher than the theoretical value calculated based on the density of LiTFSI, comparing the volume and *Z*-direction size of the fully relaxed composite configurations, no significant expansion or contraction was observed in the model with the highest LiTFSI/iCOF ratio (Figure S4). In this study all of the MD simulation were performed by LAMMPS with identical relaxation parameters.[29]

The Polymer Consistent Force Field (PCFF+) was used to describe the interactions between atoms.[30,31] This force field includes a wide range of chemical elements and has been successfully applied in polymer electrolyte simulations.[32,33] In this model, electrostatic interactions are described using point charges, which tend to overestimate the forces between cations and anions, resulting in calculated diffusion coefficients that are significantly lower than experimental values. A classical approach in polymer electrolyte simulations is to reduce the partial charges on the ionic atoms to 0.7 times their original values,[34,35] which has been effectively applied in PEO/LiTFSI systems.[36] The charges of all types of atoms in MD models are listed in Table S1 and Figure S5. Nevertheless, the calculated diffusion coefficient is still underestimated, making it challenging to derive the diffusion coefficient and conductivity accurately at room temperature from the linear regime of the MSD data. Therefore, we conducted molecular dynamics simulations at elevated temperatures, a common approach to accelerate the study of ionic transport properties. At 473 K, we calculated the conductivity of pure iCOF to be $7.7912 \times 10^{<M->5}$ S/cm (Figure S6), and the experimental value of conductivity for pure iCOF is $2.70 \times 10^{<M->5}$ S/cm at 298 K.[23] Detailed data can be found in the Supporting Information (Figure S8).

To obtain stable configurations of iCOF-based composite electrolytes, we performed relaxation in multiple stages. Prior to relaxing the entire model, we conducted a 1 ns local NVT simulation of the substances within the iCOF channels, including $TFSI^-$, SO_3^-, and Li^+. During the subsequent relaxation of the entire model, 2 ns of NVT simulation and 4 ns of NPT simulation were performed, after which the volume and density of all models converged, indicating that relaxation was complete (Figure S3). Based on this, we conducted a 40 ns NVT simulation to calculate MSD data and output the trajectories of all atoms for further analysis. The flow chart of the MD simulations can be found in the Supporting Information (Figure S2). The ion diffusion coefficients were computed from the MSD data, and the ion migration energy barriers were determined based on the diffusion coefficients at different temperatures using the Arrhenius equation. Relative equations can be found in Section 2 in the Supporting Information. From the atomic trajectory data, we calculated the radial distribution functions (RDF) and coordination numbers (CN) centered on Li^+.

Based on RDF and atomic trajectory data, the local environment of Li+ was analyzed by calculating configuration entropy and bond order orientational parameters. BOO is often quantified using spherical harmonics, which are mathematical functions that describe the angular dependence of a system's properties. The bond vectors between a central atom and its neighbors are projected onto spherical harmonics, and the resulting coefficients provide a set of BOO parameters, typically denoted as q_l or $\overline{q}_1$, where l is the order of the spherical harmonics. For a given atom, the BOO parameter is calculated by averaging the spherical harmonic functions over all bonds (neighboring atoms):

$$q_l = \left(\frac{4\pi}{2l+1} \sum_{m=-l}^{l} \left| \frac{1}{N_b} \sum_{j=1}^{N_b} Y_{lm}(\theta_{ij}, \emptyset_{ij}) \right| \right)^{1/2}$$

where $N_b$is the number of bonds (neighboring atoms). $Y_{lm}(\theta_{ij}, \emptyset_{ij})$ are the spherical harmonics functions. $\theta_{ij}, \emptyset_{ij}$ are the polar and azimuthal angles of the bond vector between the central atom and neighbor *j*.[37]

In this work, we find the neighbors with an adaptive cutoff radius. For atom *i*, its cutoff radius r_{cut} is calculated as:

$$r_{cut}(i) = P \times \left(\frac{1}{N_b} \sum_{j=1}^{N} r_{ij} \right)$$

First, the average distance of *N* nearest atoms is calculated, and then this distance is multiplied by a padding factor *P*. In this work, N_b is 6 and *P* is 1.2. These two parameters are chosen to include all the atoms within the distance to the first peak of the radial distribution function.

Conflict of Interests

The authors declare no conflict of interest.

Data Availability Statement

The data that support the findings of this study are available from the corresponding author upon reasonable request.

Keywords: Solid state electrolytes · Ionic covalent organic frameworks · Molecular dynamics · Ion transport mechanisms · Lithium-ion batteries

[1] M. Li, J. Lu, Z. Chen, K. Amine, *Adv. Mater.* **2018**, *30*, 1800561.
[2] J. Xie, Y.-C. Lu, *Nat. Commun.* **2020**, *11*, 2499.
[3] F. Wu, J. Maier, Y. Yu, *Chem. Soc. Rev.* **2020**, *49*, 1569–1614.
[4] S. Randau, D. A. Weber, O. Kötz, R. Koerver, P. Braun, A. Weber, E. Ivers-Tiffée, T. Adermann, J. Kulisch, W. G. Zeier, F. H. Richter, J. Janek, *Nat. Energy* **2020**, *5*, 259–270.
[5] Manthiram, X. Yu, S. Wang, *Nat. Rev. Mater.* **2017**, *2*, 16103.
[6] K. J. Kim, M. Balaish, M. Wadaguchi, L. Kong, J. L. M. Rupp, *Adv. Energy Mater.* **2021**, *11*, 2002689.
[7] T. Ye, L. Li, Y. Zhang, *Adv. Funct. Mater.* **2020**, *30*, 2000077.
[8] Y. Hu, J. M. Whiteley, S. Wan, Y. Jin, S. H. Lee, W. Zhang, *J. Am. Chem. Soc.* **2019**, *141*, 7518–7525.
[9] K. Jeong, S. Park, G. Y. Jung, S. H. Kim, Y. H. Lee, S. K. Kwak, S. Y. Lee, *J. Am. Chem. Soc.* **2019**, *141*, 5880–5885.
[10] K. T. Tan, S. Ghosh, Z. Wang, F. Wen, D. Rodríguez-San-Miguel, J. Feng, N. Huang, W. Wang, F. Zamora, X. Feng, A. Thomas, D. Jiang, *Nat. Rev. Methods Primers* **2023**, *3*, 1.
[11] A. P. Côté, A. I. Benin, N. W. Ockwig, M. O'Keeffe, A. J. Matzger, O. M. Yaghi, *Science* **2005**, *310*, 1166–1170.
[12] Y. Du, J. M. Whiteley, H. Yang, S. Wan, Y. Jin, S. H. Lee, W. Zhang, *Angew. Chem. Int. Ed.* **2016**, *55*, 1737–1741.
[13] W.-H. Huang, X.-M. Li, X.-F. Yang, X.-X. Zhang, H.-H. Wang, H. Wang, *Mater. Chem. Front.* **2021**, *5*, 3593–3613.
[14] X. Liang, Y. Tian, Y. Yuan, Y. Kim, *Adv. Mater.* **2021**, *33*, 2105647.
[15] Y. Cao, M. Wang, H. Wang, C. Han, F. Pan, J. Sun, *Adv. Energy Mater.* **2022**, *12*, 2200057.
[16] Z. Li, Z. W. Liu, Z. J. Mu, C. Cao, Z. Li, T. X. Wang, Y. Li, X. Ding, B. H. Han, W. Feng, *Mater. Chem. Front.* **2020**, *4*, 1164–1173.
[17] X. He, Y. Yang, H. Wu, G. He, Z. Xu, Y. Kong, L. Cao, B. Shi, Z. Zhang, C. Tong, K. Jiao, K. Zhu, Z. Jiang, *Adv. Mater.* **2020**, *32*, 2001284.
[18] H. Y. Dunlap, S. Wan, J. M. Whiteley, S. Lee, W. Zhang, *J. Am. Chem. Soc.* **2019**, *141*, 7518–7525.
[19] D. A. Vazquez-Molina, G. S. Mohammad-Pour, C. Lee, M. W. Logan, X. Duan, J. K. Harper, F. J. Uribe-Romo, *J. Am. Chem. Soc.* **2016**, *138*, 9767–9770.
[20] D. Dong, H. Zhang, B. Zhou, Y. Sun, H. Zhang, M. Cao, J. Li, H. Zhou, H. Qian, Z. Lina, H. Chen, *Chem. Commun.* **2019**, *55*, 1458–1461.
[21] J. Chen, J. Zhang, X. Wang, N. Fu, Z. Yang, *Electrochim. Acta.* **2023**, *449*, 142267.
[22] Z. Guo, Y. Zhang, Y. Dong, J. Li, S. Li, P. Shao, X. Feng, B. Wang, *J. Am. Chem. Soc.* **2019**, *141*, 1923–1927.
[23] J. Huang, L. Cheng, Z. Zhang, C. Li, K.-T. Bang, A. Liem, H. Luo, C. Hu, Y.-M. Lee, Y. Lu, Y. Wang, Y. Kim, *Adv. Energy Mater.* **2024**, *14*, 2400762.
[24] H. Zhang, F. Chen, J. Carrasco, *Energy Storage Mater.* **2021**, *36*, 77–90.
[25] K. Zhang, B. Zhang, M. Weng, J. Zheng, S. Li, F. Pan, *Phys. Chem. Chem. Phys.* **2019**, *21*, 9883–9888.
[26] C. Wang, T. Ouyang, X. Wang, S. Liu, G. Tian, F. Fan, P. Liu, S. Wang, C. Zeng, C. Shu, *J. Energy Chem.* **2024**, *99*, 384–392.
[27] MedeA-3.5, Materials Design, Inc., San Diego, CA, USA, **2022**. <
[28] F. Zhang, L. Cheng, M. Wu, X. Xu, P. Wang, Z. Liu, *Energy Convers. Manag.* **2020**, *221*, 113159.
[29] S. Plimpton, *J. Comput. Phys.* **1995**, *117*, 1–19.
[30] H. Sun, *J. Comput. Chem.* **1994**, *15*, 752–768.
[31] D. Rigby, H. Sun, B. E. Eichinger, *Polym. Int.* **1997**, *44*, 311–330.
[32] A. France-Lanord, J. C. Grossman, *Phys. Rev. Lett.* **2019**, *122*, 136001.
[33] N. Molinari, J. P. Mailoa, B. Kozinsky, *Chem. Mater.* **2018**, *30*, 6298–6306.
[34] T. G. A. Youngs, C. Hardacre, *ChemPhysChem* **2008**, *9*, 1548–1558.
[35] R. M. Lynden-Bell, T. G. A. Youngs, *J. Phys. Condens. Matter.* **2009**, *21*, 424120.
[36] A. France-Lanord, Y. Wang, T. Xie, J. A. Johnson, Y. Shao-Horn, J. C. Grossman, *Chem. Mater.* **2020**, *32*, 121–126.
[37] Y. Deng, Y. Wang, K. Xu, Y. Wang, *J. Chem. Theory Comput.* **2023**, *19* (22), 8332–8339.

Manuscript received: August 31, 2024
Revised manuscript received: December 8, 2024
Version of record online: December 17, 2024